Available online at www.sciencedirect.com

ScienceDirect

Procedia Manufacturing 26 (2018) 871–879

Procedia MANUFACTURING

www.elsevier.com/locate/procedia

46th SME North American Manufacturing Research Conference, NAMRC 46, Texas, USA

Implementation of Advanced Laser Control Strategies for Powder Bed Fusion Systems

H. Yeung [a]*, B.M. Lane [a], M. A. Donmez [a], J.C. Fox [a], J. Neira [b]

[a] *Engineering Laboratory,* [b] *Physical Measurement Laboratory, National Institute of Standards and Technology, Gaithersburg, MD 20899*

* Corresponding author. Tel.: +1-301-975-2786
E-mail address: ho.yeung@nist.gov

Abstract

Laser path, scan speed, and laser power are critical machine parameters for determining the quality of the output of laser-based powder bed fusion (LPBF) processes. A jerk-limited control strategy is implemented for laser path planning on a LPBF additive manufacturing (AM) testbed. The actual and commanded laser paths/velocities are found to be in better agreement with each other compared to conventional controls. The new controller enabled implementation of advanced laser power control strategies synchronized with laser position and velocity by embedding all into a modified G-code (referred as AM G-code). An interpreter is developed to utilize sophisticated LPBF laser control commands.

Peer-review under responsibility of the scientific committee of the 4th International Conference on System-Integrated Intelligence.

Keywords: Laser Powder Bed Fusion Additive Manufacturing (LPBF AM), Scan Strategies, AM G-code, Jerk-limited Control

1. Introduction

Laser powder bed fusion (LPBF) is an additive manufacturing (AM) process in which a focused, high power laser selectively melts geometric patterns into layers of metal powder, ultimately building a near fully dense freeform part [1]. The LPBF fabrication process, and the resulting part quality, are influenced by hundreds of controlled and uncontrolled process parameters [2]. To form fully dense parts, laser position, velocity, and power must be well controlled based on the powder layer characteristics (material, density, thickness, etc.) to adequately fuse adjacent scan tracks and previous layers. Improper combination of these parameters can cause defects that plague LPBF parts. Pores, for example, have been attributed to various phenomena related to the laser power-velocity profiles or scan strategies (e.g., keyholing and pore entrapment at high laser energy densities [3]), or insufficient re-melting of adjacent scan tracks, often called 'lack of fusion' [4–6]. Better controlled velocity or power profiles, or power density, along each scan

2351-9789
Peer-review under responsibility of the scientific committee of the 4th International Conference on System-Integrated Intelligence.
10.1016/j.promfg.2018.07.112

path can reduce the probability of defect formation, or provide a parametric space for process optimization [7,8].

The laser control for LPBF systems involves both laser path and laser power. A focused laser spot is directed to the powder bed by a pair of mirrors driven by galvanometer (galvo) motors, therefore laser path control is achieved by controlling the two galvo motors in a coordinated manner. Laser power is electronically adjusted through the laser amplifier, usually by a digital 'gate' signal to turn the laser on/off, and a low-voltage analog signal proportional to laser power. Most commercial scanning systems, both standalone and integrated into LPBF machines, use a step velocity profile for motion control. Step velocity assumes infinite acceleration, making it impossible for the mirrors to truly follow a command. Therefore, temporal and spatial accuracy are compromised leading to geometric inaccuracies and material defects.

The National Institute of Standards and Technology (NIST) is constructing an open architecture Additive Manufacturing Metrology Testbed (AMMT) [9] to study advanced process monitoring and control strategies. The work described here is used to implement the laser control on the AMMT. The AMMT is instrumented with a high-speed camera coaxially aligned with the laser for *in-situ* melt-pool imaging. Laser position and power are measured at 100 kHz from the galvo position feedback and laser source unit, respectively [10]. All experiments in this paper were conducted on the NIST AMMT.

2. Influence of laser control on scan path accuracy

In numerical control of machine tools, a jerk-limited path is usually used to avoid excitation of vibration modes in the mechanical structure [11,12]. A jerk-limited path has a smooth velocity profile which is more easily followed by a physical system, and results in better spatial and temporal path accuracy. Here, spatial accuracy refers to geometric position of the laser spot, and temporal accuracy refers to the spot reaching designated positions at the designated time. Temporal accuracy is not usually a concern for machine tools. However, for advanced LPBF scan strategies incorporating line-to-line or within-line velocity or power control, both temporal and spatial accuracy are essential. To accomplish this, jerk-limited motion control is implemented on the NIST AMMT.

2.1. Jerk-limited path design

A sine function is chosen for the jerk. Jerk is the time derivative of acceleration, therefore can be integrated with boundary conditions to get the path (position) profile, *x(t)*, where *t* is the time. The detail equations are given below:

$$j(t) = K \cdot sin(\omega t) \tag{1}$$

j(t) is the jerk, K is its amplitude, ω is its angular velocity

$$a(t) = \int j(t)\, dt = -\frac{K}{\omega}\cos(\omega t) + C \tag{2}$$

a(t) is the acceleration, C is a constant; at $t = 0$, $a(t) = 0$, $C = K/\omega$.

$$v(t) = \int a(t)\, dt = -\frac{K}{\omega^2}\sin(\omega t) + \frac{Kt}{\omega} + D \tag{3}$$

v(t) is the velocity, *D* is a constant; at $t = 0$, $v(t) = 0$, $D = 0$.

$$x(t) = \int v(t)\, dt = \frac{K}{\omega^3}\cos(\omega t) + \frac{Kt^2}{2\omega} + E \tag{4}$$

x(t) is the position, *E* is a constant; at $t = 0$, $x(t) = 0$, $E = -K/\omega^3$. Setting a constraint of maximum acceleration, *A*, allowed on the system using Eq. 2 yields:

$$\frac{2K}{\omega} = A \tag{5}$$

At $t = 2\pi/\omega$, set $v(t) = F$, where F is the feed rate. From Eq. 3

$$\frac{2K\pi}{\omega^2} = F \tag{6}$$

Solving Eq. 5 – 6 for ω and K, the path equation will be

$$x(t) = \frac{F^2}{2A\pi}\cos\left(\frac{A\pi t}{F}\right) + \frac{At^2}{4} - \frac{F^2}{2A\pi} \tag{7}$$

2.2. Path planning comparison

Nine square laser scan paths (each consisting of four sequential moves along the sides of a 4 mm by 4 mm square) were generated on the AMMT using different motion control parameters (Table 1). Laser power is a constant 100 W. For the step velocity profile, a wait time was introduced after each move to improve spatial path accuracy, emulating commercial controllers.

Table 1. Parameter settings for squares scanned with different motion controls. The step velocity is simulated by a 100 000 m/s2 acceleration.

Scan #	Velocity Profile	Max. Acc.	Wait time
1	Sine vel. (Jerk-limited)	1000 m/s^2	0 s
2	Sine vel. (Jerk-limited)	5000 m/s^2	0 s
3	Sine vel. (Jerk-limited)	100 000 m/s^2	0 s
4	Ramp vel.	1000 m/s^2	0 s
5	Ramp vel.	5000 m/s^2	0 s
6	Ramp vel.	100 000 m/s^2	0 s
7	Step vel. with wait time	100 000 m/s^2	0.002 s
8	Step vel. with wait time	100 000 m/s^2	0.005 s
9	Step vel. with wait time	100 000 m/s^2	0.0005 s

The image of the scan tracks is shown in Fig. 1a, and the commanded and measured scan paths are plotted in Fig. 1b, with scan numbers marked on the figures. The distortion of the scanned squares occurs when the next move starts before the current destination can be reached. A carefully calibrated wait time can be introduced to compensate this distortion, such as shown in scan 7. However, this wait time improves only geometric accuracy and it is velocity sensitive (Sec. 4). If it is too long, it will cause over melting (Fig. 1a scan 8, red arrows). If it is too short, it cannot fully compensate the distortion (scan 9).

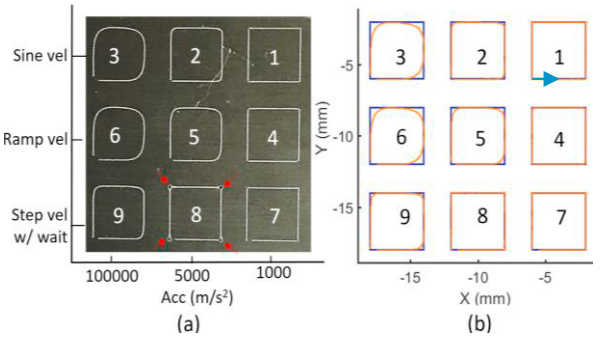

Fig. 1. Square scan paths generated with different motion controls. (a) Image of the scan tracks on an aluminum plate. Note the acceleration scale does not apply to step velocity. (b) X-Y plot of the scan paths. Blue is the command; orange is the measured. The scan is in counter-clockwise direction. The blue arrow marks the first side scanned.

The commanded and measured x-axis position *x(t)*, velocity *v(t)*, and acceleration *a(t)* for scans 1, 4, and 7 in Table 1 are plotted in Fig. 2. Step velocity requires an impulse acceleration, which is unrealistic on any physical system, and shows the greatest deviation from the commanded path. Ramp velocity is much better followed except at the corners. Sine velocity (jerk-limited) is best followed. Wait time can be added in all cases to improve spatial accuracy, but has no effect on temporal accuracy.

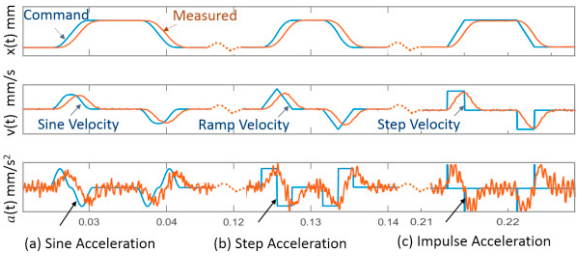

Fig. 2. Position *x(t)*, velocity ($v(t) = dx(t)/dt$), and acceleration ($a(t) = dv(t)/dt$) plotted against time for galvo x axis. Blue is the command; orange is the measured.

2.3. Temporal accuracy of scan path

To visualize the effect of temporal path accuracy, two series of 2 mm x 2 mm patterns were scanned on an aluminum plate at different speeds (200 mm/s to 2000 mm/s) with jerk-limited and step velocity motion controls. Constant build speed, constant power modes (section 4.1) were used; hence the laser power turns on and off at designated positions. Acceleration for jerk-limited control was set to 1000 m/s^2. Wait time for step velocity control was calibrated at speed of 200 mm/s. Figure 3 shows the scan tracks on the aluminum plate. The gaps in the scanned patterns for step velocity control indicate the laser spot did not reach the designated position at the designated time (i.e., a temporal error). No gap was observed for jerk-limited control at all speeds.

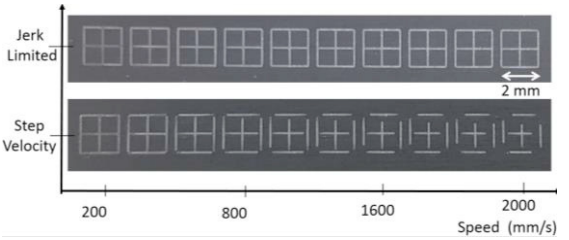

Fig. 3. Comparison of jerk-limited and step velocity motion control at different speeds.

3. Influence of laser control on LPBF process

Laser power and scan speed influence the input energy density, and any errors resulting from control lead to non-uniformities in process characteristics, potentially causing material defects. Since one key signature of process characteristics is the geometry (size and shape) of the melt-pool, one can observe the

melt-pool to study the influence of laser control on the process. To measure melt-pool geometry, a high-speed camera was setup coaxially with the laser beam using a dichroic mirror, imaging lens, and filter. Emitted light from the melt-pool, which is filtered at 850 nm (40 nm bandwidth), is imaged on the camera sensor with nominal 1:1 magnification and 12 μm pixel size. The camera is set to 30 000 frames/s, 31.6 μs exposure time, 256 pixel x 256 pixel window, and 8-bit dynamic range (grayscale). The gray levels are used to relate to melt-pool dimensions [13]. Contours, representing isotherm lines, can be drawn on the raw melt-pool image to represent equal intensity (Fig. 4). A contour with intensity digital level of 170 was found to equate to the physical melt pool width based on the ex-situ measured scan track width via microscope inspection. This digital level contour is then used to infer melt pool boundary from the high-speed images and calculate melt pool dimensions and area.

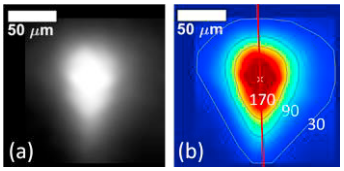

Fig. 4. Melt-pool image analysis. (a) raw grayscale image. (b) processed image. Black contour lines show different intensity levels (DL); red line shows melt-pool orientation.

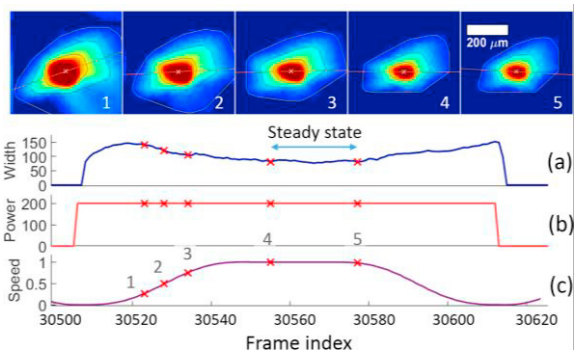

Fig. 5. A single-track scan on stainless steel. (a) Melt-pool width (μm) measured from in-situ melt-pool images. (b) Commanded laser power (W). (c) Commanded laser speed (m/s). Melt-pool images corresponding to the marked locations (1-5) are shown on the top.

An example of using in-situ melt-pool imaging to study the effects of laser control on melt-pool geometry is shown in Fig. 5. A single track was scanned on stainless steel and monitored using the co-axial high-speed camera. The melt-pool width measured from images is plotted together with commanded laser power and laser speed (Fig. 5a – 5c). The images at speed = 0.25 m/s, 0.5 m/s, 0.75 m/s, and 1 m/s are shown on top of the plots, with their respective locations (1-5) marked. It can be seen from Fig. 5a that melt-pool width decreases as speed increases (1-4), and is relatively constant at constant speed (4-5). For a uniform process, the melt-pool size must be kept constant, which can be achieved by changing the laser power in coordination with the instantaneous velocity and position of the scan. For such coordination, high temporal accuracy of scan velocity is required.

4. LPBF scan strategies and implementation by G-code

The jerk-limited path planning makes it possible to develop complicated scan strategies, which require precise time-velocity and time-position relationship. Such strategies include modulating laser power with instantaneous velocity to achieve constant power density, or modulating power with instantaneous location to respond to dynamic thermal effects stemming from heat accumulation due to local variations in part geometry or scan history. The melt-pool continuity may also be important. The on/off modulation of the laser and dramatic variation of laser power or speed can perturb a nominally steady-state melt-pool. A more ‘smooth’ build may be possible if there are reduced power and speed variations. To facilitate the test and implementation of complicated scan strategies, we proposed the concept of laser path modes and laser power modes [10], and implemented them through a modified version of G-code (referred as AM G-code).

4.1. AM G-code

G-code is a high-level programming language for computer numerical control (CNC). An EIA standard for G-code can be found in [14]. A simple G-code line such as ‘G01 X1 Y1 F1000’ commands the machine tool to move linearly (G01) from current position to x-y coordinate (1, 1), with steady state feed (F) of 1000 (mm/s). Such a ‘move’ is interpolated by G-code interpreter into a sequence of digital positions (micro-steps sent to motor controller) based on the velocity profile and the path mode. The path mode defines how sequential moves are planned. For example, for a rectangular path such as in Fig. 1, the current move can stop completely before next move; or it can continue

to next move through a connection arc. Hence for same G-code, different paths can be interpreted based on different path modes.

Conventional G-code (and M-code) does not support power control within a move. The AM G-code is developed by adding a keyword 'L' to specify the laser power level. The usage of L is similar to the keyword F (feed). Power mode is also defined and together with L to describe the laser power profile within a move. A summary of laser path and power modes defined for AM G-code is listed below.

4.2. AM G-code interpretation modes

Three laser path modes and three laser power modes are defined. A combination of both can be used to fully describe the power-velocity-position strategy.

Laser path modes
1) Exact stop – complete stop at the end of each move.
2) Constant build speed – keep speed constant while laser is on.
3) Continuous – match the end and start velocity of two moves.

Laser power modes
1) Constant power – keep laser power constant during each move.
2) Constant power density – keep power/speed ratio constant.
3) Thermal adjusted – adjust power per predefined/ determined thermal properties or feedback from real-time monitoring.

One laser path mode and one or multiple (such as constant power density + thermal adjusted) laser power modes can be set for interpretation - hence the same AM G-code script can be interpreted into different scan strategies. As an illustration, a matrix of nine 2 mm x 1.5 mm rectangular areas was interpreted with the 3x3 combinations of the laser path and power modes (Fig. 6-7). The areas are filled by a hatching pattern (rastering) of 0.2 mm spacing and 45° inclination angle. The color bars in the figures indicate laser speed and power, respectively. The scan sequence is numbered 1–9. The constant build speed mode is implemented by allowing the overshoot of the path but with laser power turned off; the continuous mode replaces the sharp corner with an arc; the constant power density mode maintains constant power-to-velocity ratio; and the thermal adjusted mode by inversely proportion power to 'proximity'. 'Proximity' definition is based on the distance from the neighborhood points already scanned. Similarly, thermal adjusted mode can also be implemented based on local geometry and heat conduction (section 4.3). The usage of laser power keyword L is further illustrated in path 6 (Fig. 7), where L200 (laser power = 200 W) was set for all linear moves and L100 was set for the connection arcs.

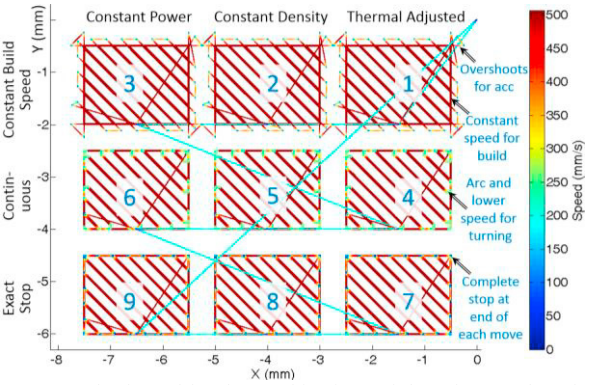

Fig. 6. Path planned by the combinations of three laser path and three laser power modes. Laser speed is represented by color.

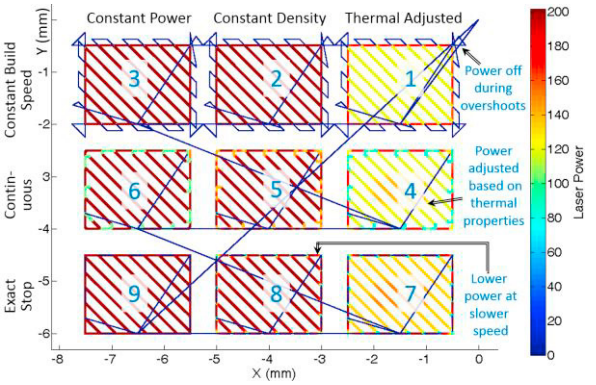

Fig. 7. Path planned by the combinations of three laser path and three laser power modes. Laser power is represented by color.

4.3. Implementation of thermal adjusted mode

The thermal adjusted mode demonstrated in Fig. 6-7 is based on a single layer residual heat compensation model. The similar concept can be extended to more complicated multiple-layer builds such as the overhanging structure (a bridge) shown in Fig. 8a. Overhanging structure is problematic to build because the large variation in thermal conductivities between powder and solidified regions. Traditionally this is addressed by either adding support structures to improve the local thermal conductivity [15], or changing the structure design itself [16]. The thermal adjusted mode proposed here provides a framework to handle such issues through fine tuning of laser power

and velocity at each scan point. Since it operates at G-code interpretation level, it is independent of the structure design, and hence a more generic solution. A unitless geometric-based thermal conduction factor (GCF) is developed in the interpreter which is conceptually demonstrated in Fig. 8.

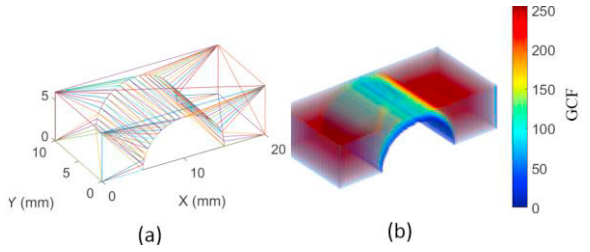

Fig. 8. Thermal adjusted mode implementation. (a) STL plot of a bridge structure. (b) Geometric conductivity factor (GCF) model constructed from the scan path.

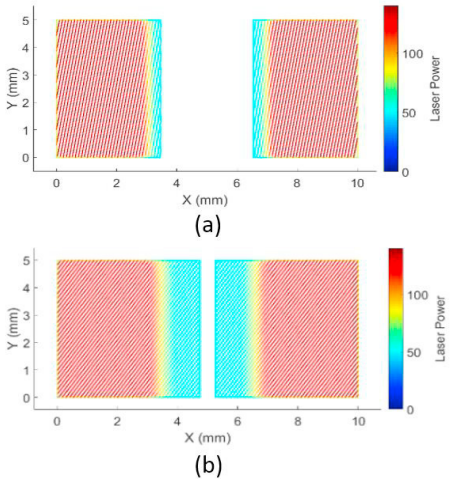

Fig. 9. Scan power at (a) 200th layer. (b) 250th layer. The laser power is reduced gradually at the overhanging area.

The x-y scan positions generated by the G-code interpreter for the part in Fig. 8a are used to create a layer-wise bitmap for the 'melted' pixels. A pixel is 'melted' if it is within a specified distance of the laser spot center at a 'laser on' scan point. Depending on the pixel size defined (10 µm by 10 µm pixel is used here), a relatively precise cross section of the part being built can be modeled. These bitmap layers are then added up layer by layer, and a GCF value is assigned to the current pixel based on the weighted GCF value of the already-built pixels (from previous layer and its same layer neighbors) with immediate contact to it. Pixels on the base plate (0^{th} layer) have a full GCF value. A weighing factor is based on a hypothetical cylinder with diameter approximately equal to melt pool width, and depth equal to powder layer. For example, a 100 µm melt-pool and 25 µm layer results in a 50 % weight to the previous layer since ratio of the bottom surface area to side surface area is about 50 : 50.

A multi-layer GCF model (or a three-dimensional GCF lookup table) can hence be built. Fig. 8b shows such a model for the object in Fig. 8a. Once this model is built, the laser power at each scan point can be adjusted according to the GCF value at that location. A linear function $L = L_o (aX+b)$ can be used to adjust the laser power, where L is the adjusted laser power, L_o is the original laser power, X is the normalized GCF, a and b are constants which can be optimized from experiments. Figure 9 shows the adjusted laser power at different layers for the bridge structure in Fig. 8. Note the gradually decreasing power level when approaching the overhanging region.

5. Comparison of different scan strategies

A key signature characteristic in LPBF AM processes is the melt-pool geometry. It is used to compare the effects of different scan strategies in this study. In-situ high-speed coaxial imaging is used to measure the melt-pool image area, and ex-situ confocal microscopy is used to measure the surface topology of the solidified melt-pool (scan track).

5.1. Melt-pool image area

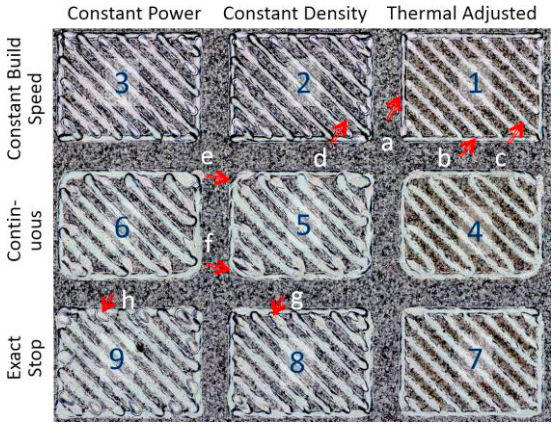

Fig. 10. Path planned by the combinations of three laser path and three laser power modes. Image shows the scan on a stainless-steel plate.

The paths planned in Fig. 6-7 were scanned on a stainless-steel plate. The images of the scanned areas in Fig. 10 provide an overview of the effect of different scan modes. The result from in-situ melt-pool size

analysis is given in Fig. 11, with camera images demonstrated from locations 'a' to 'h' marked on both Fig. 10 and 11. The melt-pool image area is plotted together with laser power and scan speed. For constant build speed mode (1-3), the laser was turned on and off at very precise locations. No laser marks outside the rectangles are visible, and no gap at the connection of the scan tracks are observed. The power-velocity-position is well coordinated under jerk limited motion control. Constant build speed mode has the most even melt-pool size. Continuous mode (4-6) creates a continuous melt-pool. But, the irregularity in the melt-pool image area will require further effort to improve. Exact stop constant power mode (9) shows the biggest variation of melt-pool size. However, the melt-pool is much more consistent in the exact stop constant density mode (8) and exact stop thermal adjusted mode (7), proving the power adjustment can effectively suppress the melt-pool irregularity. The thermal adjusted mode (1, 4, 7) has demonstrated the benefit of implementing more advanced scan strategies. The overshoots in melt-pool image area are reduced (e.g., comparing 7 to 8 and 9). The track width for 1, 4, and 7 are more uniform. A similar concept can be applied to overhanging structures, thin wall structures, etc. in 3D geometry to compensate for the varying local thermal conduction.

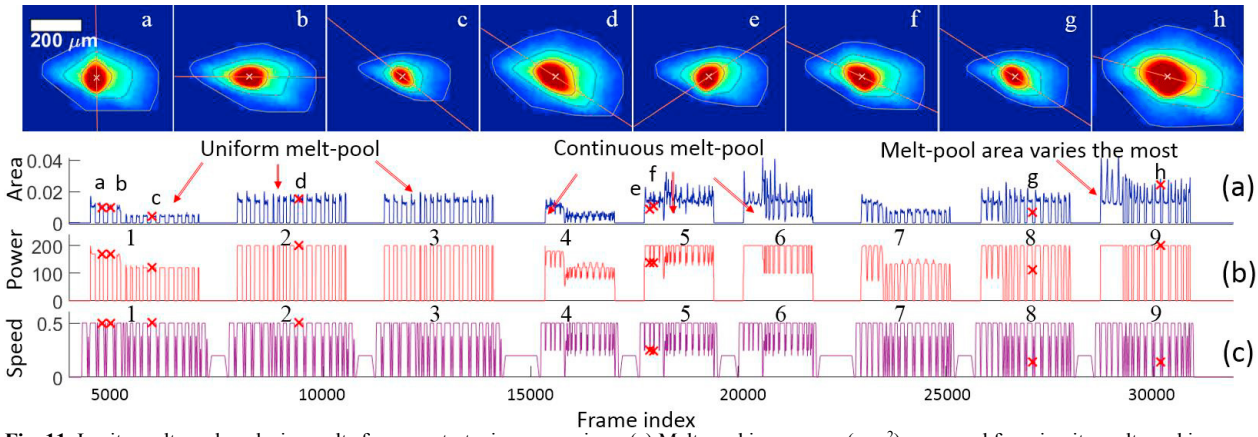

Fig. 11. In-situ melt-pool analysis results for scan strategies comparison. (a) Melt-pool image area (mm^2) measured from in-situ melt-pool images. (b) Commanded laser power (W). (c) Commanded laser speed (m/s). Melt-pool images corresponding to the marked locations (a-h) are shown on the top.

5.2. Scan track surface topology

Confocal microscopy enables the reconstruction of three-dimensional surfaces from a set of images obtained at different focal depths. It was used to compare the surface topology of the scan tracks resulted from various laser path modes. Figure 12 shows images of three single tracks scanned on a metal plate with exact stop, constant build speed, and continuous path modes, respectively. The laser power was constant mode at 200 W, and the nominal laser speed was 500 mm/s. The corresponding confocal microscopic measurements are plotted in Fig. 13. Figure 13a is the height profiles measured along the scan tracks, Fig. 13b is the surface topology of the scan track at various locations marked by the red dotted lines in Fig. 13a. A bump and a hole are clearly visible for exact stop and constant build speed modes, at the positions when the laser power was turned on / off. This agrees very well with the melt flow simulation in [6]. The hole is deeper for constant build speed mode, likely due to the fact that the laser was still travelling at high speed when it was turned off. However, this does not seem to have the same effect when the laser was turned on - the heights of the bumps for constant build speed and exact stop modes are similar. There are very little variations in the scan track heights for the continuous mode. Comparing Fig. 13 and Fig. 11, it is interesting to see constant build speed mode has the most uniform melt-pool image area but the largest variation in scan track height at the end points. On the other hand, continuous mode has the largest variation in melt-pool image area but most uniform scan track height.

The variation of track height is mainly due to the laser power switching on and off, which is the most frequent and drastic (while the laser is travelling at full speed) in constant build speed mode. The variation of

melt-pool image area is mainly due to the changes of laser speed, power and direction. Constant build speed mode turns off laser power when direction changes or speed slows to minimize melt-pool area variation. Continuous mode, on the other hand, keeps laser power on all the time to minimize track height variation. If the goal is to keep both the height and area variations minimum, a combination of continuous path mode and constant power density mode seem the best choice. However, the melt-pool dynamic is very complicated, constant power density alone cannot guarantee a constant melt-pool area. Many other factors, such as thermal properties, powder dimension, gas flow, etc. can all affect the build quality. Ongoing studies are needed to continuously optimize the control parameters based on the framework proposed here.

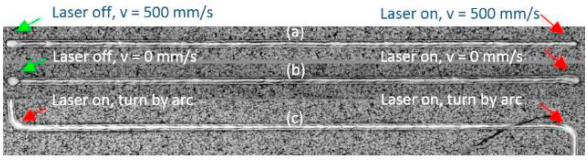

Fig. 12. Single track scan with (a) exact stop, (b) constant build speed, and (c) continuous laser path mode.

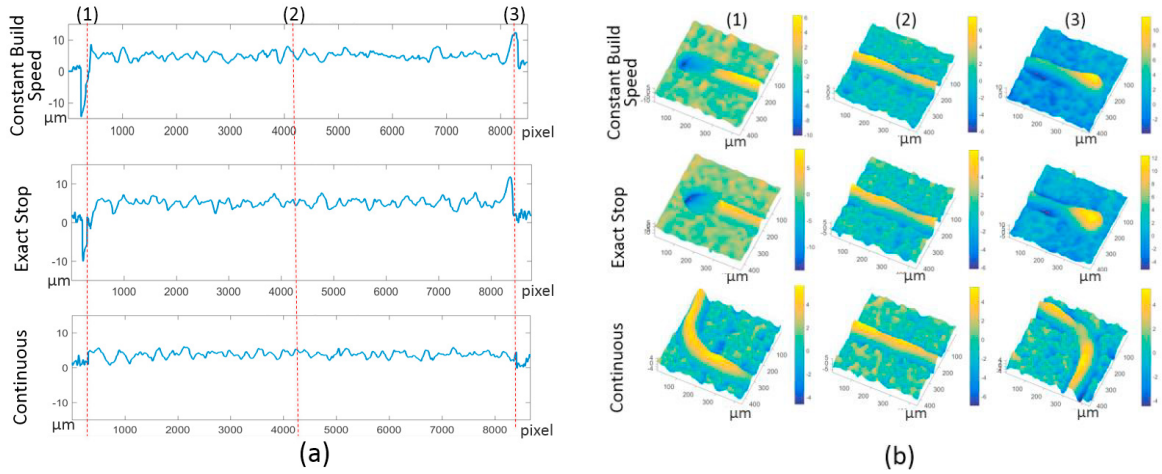

Figure 13. Confocal microscopic measurements. (a) Height profile along the melt-track. (b) The surface topographies at the locations indicated by red dotted lines in (a).

6. Discussion and summary

A jerk-limited motion control was implemented on a LPBF AM testbed, and improved position and velocity temporal accuracies were demonstrated. This enabled the implementation of advanced laser control strategies based on precise power-velocity-position coordination. Such strategies were proposed and implemented through 'AM G-code' with three laser path modes and three laser power modes built into its interpreter. A thermal-adjusted mode was also proposed that locally varies power based on adjacent solidified material and variation in local heat conduction. Scan experiments were conducted on a metal plate to demonstrate the effectiveness of different modes, in-situ melt-pool imaging and ex-situ confocal microscopy were utilized to study the processes. The melt-pool controllability is clearly demonstrated. Experiments will be conducted for multilayer powder 3D builds to further verify their effects on the quality of the built parts. Further study is still needed to understand optimal control strategies pertaining to the AM fabrication process; however here we demonstrated methods for controllability.

References

[1] Kruth J-P, Leu M C and Nakagawa T 1998 Progress in Additive Manufacturing and Rapid Prototyping *CIRP Ann. - Manuf. Technol.* **47** 525–40

[2] Mani M, Lane B, Donmez A, Feng S, Moylan S and Fesperman R 2015 *Measurement Science Needs for Real-time Control of Additive Manufacturing Powder Bed Fusion Processes* (National Institute of Standards and Technology)

[3] King W E, Barth H D, Castillo V M, Gallegos G F, Gibbs J W, Hahn D E, Kamath C and Rubenchik A M 2014 Observation of keyhole-mode laser melting in laser powder-bed fusion additive manufacturing *J. Mater. Process. Technol.* **214** 2915–25

[4] Thijs L, Verhaeghe F, Craeghs T, Humbeeck J V and Kruth J-P 2010 A study of the microstructural evolution during selective laser melting of Ti–6Al–4V *Acta Mater.* **58** 3303–12
[5] Yadroitsev I, Thivillon L, Bertrand P and Smurov I 2007 Strategy of manufacturing components with designed internal structure by selective laser melting of metallic powder *Appl. Surf. Sci.* **254** 980–3
[6] Khairallah S A, Anderson A T, Rubenchik A and King W E 2016 Laser powder-bed fusion additive manufacturing: Physics of complex melt flow and formation mechanisms of pores, spatter, and denudation zones *Acta Mater.* **108** 36–45
[7] Zaeh M F and Ott M 2011 Investigations on heat regulation of additive manufacturing processes for metal structures *CIRP Ann. - Manuf. Technol.* **60** 259–62
[8] Antony K, Arivazhagan N and Senthilkumaran K 2014 Numerical and experimental investigations on laser melting of stainless steel 316L metal powders *J. Manuf. Process.* **16** 345–55
[9] Lane et al. Design, Developments, and Results from the NIST Additive Manufacturing Metrology Testbed (AMMT) *Solid Free. Fabr. 2016 Proc. 26th Annu. Int. Solid Free. Fabr. Symp.*
[10] Yeung H, Neira J, Lane B, Fox J and Lopez F Laser Path Planning and Power Control Strategies for Powder Bed Fusion Systems *Solid Free. Fabr. 2016 Proc. 27th Annu. Int. Solid Free. Fabr. Symp.*
[11] Erkorkmaz K and Altintas Y 2001 High speed CNC system design. Part I: jerk limited trajectory generation and quintic spline interpolation *Int. J. Mach. Tools Manuf.* **41** 1323–45
[12] Zhang Q, Li S and Guo J 2012 Smooth time-optimal tool trajectory generation for CNC manufacturing systems *J. Manuf. Syst.* **31** 280–7
[13] Rombouts M, Kruth J-P, Froyen L and Mercelis P 2006 Fundamentals of selective laser melting of alloyed steel powders *CIRP Ann.-Manuf. Technol.* **55** 187–92
[14] Electronic Industries Association Interchangeable Variable Block Data Format for Positioning, Contouring, and Contouring/Positioning Numerically Controlled Machines *EIA Stand. EIA-274- Febr. 1979*
[15] Järvinen J-P, Matilainen V, Li X, Piili H, Salminen A, Mäkelä I and Nyrhilä O 2014 Characterization of Effect of Support Structures in Laser Additive Manufacturing of Stainless Steel *Phys. Procedia* **56** 72–81
[16] Atzeni E and Salmi A 2015 Study on unsupported overhangs of AlSi10Mg parts processed by Direct Metal Laser Sintering (DMLS) *J. Manuf. Process.* **20** 500–6